This article has been accepted for inclusion in a future issue of this journal. Content is final as presented, with the exception of pagination.

A Novel Layer Jamming Mechanism With Tunable Stiffness Capability for Minimally Invasive Surgery

Yong-Jae Kim, Shanbao Cheng, Sangbae Kim, and Karl Iagnemma

***Abstract*—This paper presents a novel "layer jamming" mechanism that can achieve variable stiffness. The layer jamming mechanism exploits the friction present between layers of thin material, which can be controlled by a confining pressure. Due to the mechanism's hollow geometry, compact size, and light weight, it is well suited for various minimally invasive surgery applications, where stiffness change is required. This paper describes the concept, the mathematical model, and a tubular snake-like manipulator prototype. Various characteristics of layer jamming, such as stiffness and yield strength, are studied both theoretically and experimentally.**

***Index Terms*—Layer jamming, minimally invasive surgery (MIS), snake-like manipulator, tunable stiffness.**

I. Introduction

MINIMALLY invasive surgery (MIS) has become widely used due to its clear clinical benefits compared with open surgery. MIS patients tend to have shorter and better recoveries, and less trauma and postoperative pain. A challenge to MIS is that the dexterity of the surgeon is greatly reduced due to the use of smaller openings and long instruments, therefore, motivating the development of highly dexterous and flexible medical tools [13].

Snake-like manipulators have been investigated by many researchers for MIS applications due to their unique characteristics and advantages: high flexibility, increased safety, high dexterity, obstacle-avoidance capability, potential for miniaturization, and so on [1]–[4], [14]. Several prototypes for robotic surgery and endoscopy based on snake-like manipulators have been developed and commercialized [1]–[3]. Recently, new attempts to perform laparoscopic surgery through a single port or a natural orifice reveal that increased flexibility can hinder payload operation, despite the advantages over multiport surgery in terms of traumatic movement [4]. However, externally actuated snake-like manipulators (i.e., those with actuators located away from the manipulator structure and driven by cables or linkages) typically have an inherent disadvantage compared with angled joint manipulators (i.e., those with actuators integrated with the structure): a substantial lack of stiffness and strength.

In general, externally actuated snake-like manipulators have an underactuated structure with a compliant "backbone" [5], which often results in low stiffness at the end effector. In order to overcome this drawback, various stiffening mechanisms have been developed. One popular approach is to amplify the control wire tension and exploit the natural friction between rigid links, to modulate stiffness [2]. In practice, however, the wire tension must be high, and thus, the links must be large enough to sustain large loads. As a result, the links can occupy substantial space, and thus, it is often difficult to create a compact, lightweight manipulator based on this approach.

Recent research in the robotics community has focused on the use of tunable-stiffness materials, such magnetorheological (MR) or electrorheological fluids, to achieve variable mechanical properties. These materials can change their apparent viscosity through modulation of an external field. MR fluids have been successfully applied in robotic applications such as gripping [6] and exoskeleton actuation [7]. These technologies are most commonly used for precise control of damping and have been applied in tunable automotive suspensions. However, these materials have often limitation in achieving high stiffness or yield strength required in MIS when activated.

Phase-change materials can also be used as tunable stiffness elements in robotic devices. Previous work has involved using thermally activated materials, such as wax or solder, to create locking mechanisms in soft robotic applications, since such materials can transition between liquid and solid states [8], [9]. These methods have been shown to demonstrate large change of stiffness and strength. However, most phase-change materials (e.g., thermorheological or photorheological materials) have long activation timescales (on the order of seconds) that are not ideal for practical manipulation applications.

Particle jamming technology using granular media has recently been researched as another way to achieve tunable stiffness [10]. If each robotic joint is composed of a volume of granular material (e.g., dry sand or coffee), it can effectively transition between a fluid-like, compliant state, and a solid-like, stiff state if, for instance, a vacuum is applied on the volume such that the grains pack together to "jam" and develop a yield stress [11]. Particle jamming has interesting features such as high deformability in the fluid state and drastic stiffness increase in the solid state, without significant change in volume. However, it requires a substantial volume of granular material to achieve significant stiffness. In addition, the bulk mechanical properties of jamming are not yet well understood, and (perhaps for this reason) jamming has not yet been demonstrated as part of a practical engineering system.

Manuscript received October 31, 2012; revised December 20, 2012; accepted December 27, 2012. This paper was recommended for publication by Associate Editor S. Régnier and Editor B. J. Nelson upon evaluation of the reviewers' comments. This work was supported in part by the Samsung Advanced Institute of Technology of Samsung Electronics.

Y.-J. Kim is with the Samsung Advanced Institute of Technology, Yongin si 446-712, Republic of Korea (e-mail: yj424.kim@samsung.com).

S. Cheng is with the Direct Drive Systems, FMC Technologies, Fullerton, CA 92833 USA (e-mail: chengshanbao@gmail.com).

S. Kim and K. Iagnemma are with the Massachusetts Institute of Technology, Cambridge, MA 02139 USA (e-mail: sangbae@mit.edu; kdi@mit.edu).

Color versions of one or more of the figures in this paper are available online at http://ieeexplore.ieee.org.

Digital Object Identifier 10.1109/TRO.2013.2256313

1552-3098/$31.00 © 2013 IEEE

This article has been accepted for inclusion in a future issue of this journal. Content is final as presented, with the exception of pagination.

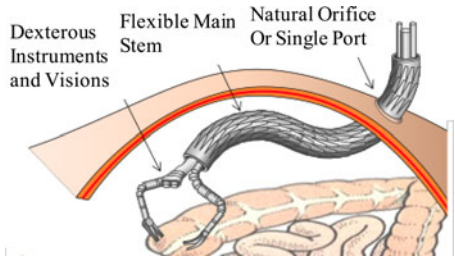

Fig. 1. Application of layer jamming mechanism: flexible main stem used for MIS.

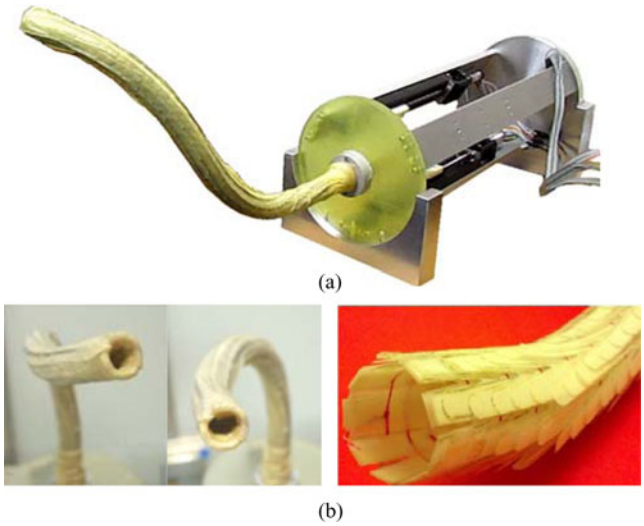

Fig. 2. (a) Prototype snake-like manipulator, including three linear actuators. (b) Closeup view of tubular shape of device with a large, central hollow section for tool passage shown on the left side, and the layer jamming scales shown on the right side.

In this paper, we propose a novel mechanism to achieve tunable stiffness termed "layer jamming," which made use of friction in between layers with the negative air pressure, along with the design of a tunable stiffness manipulator. This thin-walled tubular mechanism with tunable stiffness has several desirable properties for MIS applications, one of which is shown in Fig. 1, where the variable stiffness tubular mechanism can be used as main stem for other snake-like manipulators in MIS. Fig. 2 shows the thin-walled, tubular shape of the layer jamming mechanism. First, due to its hollow form, it can be used as a guide tube to deliver one or multiple MIS tools inside the human body. Second, during insertion of the manipulator into the body, it can assume a very flexible/low stiffness state to achieve a desired configuration and avoid accidental injury. Third, after insertion, it can be assumed that it is in a very rigid/high stiffness state to maintain a desired configuration while guiding insertion of MIS tools inside the body. A preliminary introduction of this device is published in [16], and more detailed and comprehensive study and analysis of its properties and its manufacturing process and application are presented herein as a journal article for the first time.

There are some researchers who have already made use of friction to realize the state transition between "flexible" and "rigid" of devices [17]–[19]. Our design was invented totally independently. Our design and implementation are totally different from others. We designed and developed a thin-wall, tubular manipulator consisted of a spiral form of thin plastic layer shown in Fig. 2. This spiral plastic layer [see Fig. 1(b)] is wrapped by latex rubbers to apply vacuum pressure so that friction between layers can modulate the overall stiffness of the device. Due to its unique topology of the structure, it has the desired characteristics of 1) minimum volume, 2) light weight, 3) fast state transition, and 4) high payload. The combination of these characteristics is suitable for a guiding channel in MIS. Another key difference from [19] is that Bureau *et al.* [19] only described empirical results, whereas we are presenting a rigorous analytical model with experimental validation.

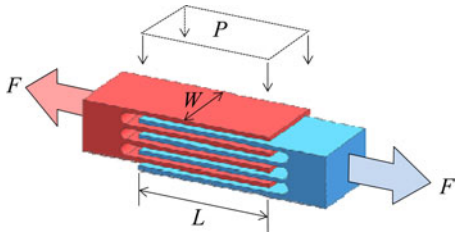

Fig. 3. Concept of layer jamming element.

Section II briefly introduces one-degree-of-freedom (1-DOF) layer jamming joint including its concept, analysis, modeling, manufacturing process, and experimental results. In Section III, the tubular snake-like manipulator is presented, and its design, actuator implementation, and experimental results and MIS application are described and discussed in detail. Section IV presents conclusions.

II. One-Degree-of-Freedom Layer Jamming Mechanism

A. Basic Concept of Layer Jamming

The basic concept of the layer jamming mechanism is illustrated in Fig. 3, where each overlapping plate represents a flap of flexible material (e.g., paper or mylar), and p, w, L, and F denote, respectively, pressure onto the outer flap, the width and length of the flaps, and the maximum resisting tensile force.

Defining the number of contact surfaces between flaps as n and the interflap frictional coefficient μ, F can be calculated as follows:

$$F = \mu\, npwL. \tag{1}$$

The resisting force can, thus, be modified by changing the number, size, or frictional properties of the overlapping flaps.

For instance, assuming that the pressure p and the size of the contacting surface of flaps wL are fixed, the resisting force can be increased by increasing the number of contact surfaces n or frictional coefficient μ. In other words, if an appropriately thin, rough material is selected, a high resisting tensile force could potentially be achieved in a compact volume. This suggests that a simple, compact mechanism could provide a significant tunable stiffness capability.

This article has been accepted for inclusion in a future issue of this journal. Content is final as presented, with the exception of pagination.

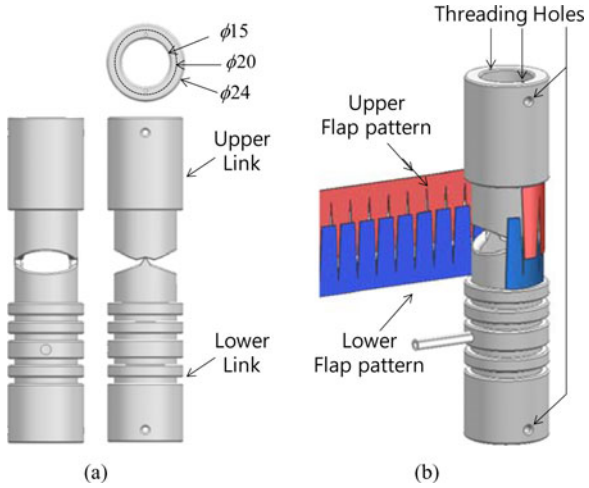

Fig. 4. (a) Layer jamming joint design. (b) Flap patterns with joint.

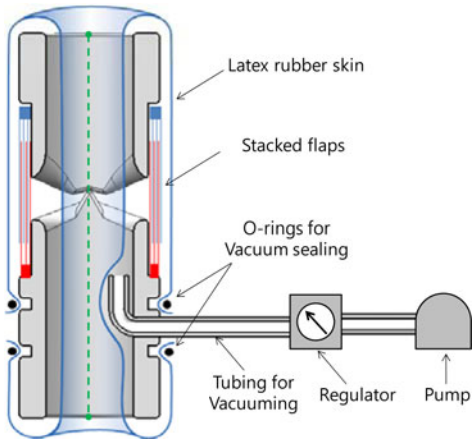

Fig. 5. Section view of assembled layer jamming joint.

B. 1-DOF Layer Jamming Joint

1) Design of 1-DOF Layer Jamming Joint: Based on the layer jamming concept, a 1-DOF joint can be designed. Fig. 3 shows a design of a 1-DOF rotational joint based on layer jamming. This is a simple pin joint, with both the upper link and lower link in Fig. 4(a) having 15 mm inner diameter and 24 mm outer diameter. A 20-mm diameter surface on both the upper and lower joint serves as a mounting surface to attach two identical patterned flaps of flexible material. These two links form a 1-DOF revolute joint that is constrained by a central tension wire (see the dotted green line in Fig. 5).

The upper flap pattern and lower flap pattern in Fig. 4(b) both have 15 mm length and 5 mm width, and a "toothed" pattern to minimize creasing or buckling during individual flap deformation. Matte surfaced Mylar film (polyethyleneterephthalate) is used for the flaps, with a thickness of 0.12 mm and measured frictional coefficient is 0.6. The stiffness of the flap material is important because the layered flaps can be subjected to compressive and bending forces according to the direction of an external applied load and can potentially fail in buckling (instead of applying a resisting force). Increasing the flap material stiffness thus increases the external load that can be tolerated before material failure.

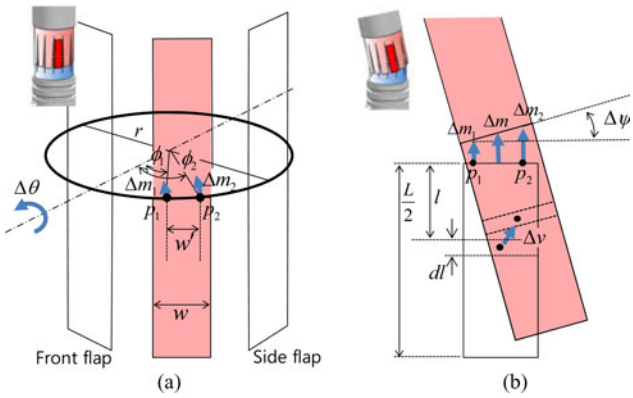

Fig. 6. Parameters of a flap at arbitrary position.

2) Manufacturing of 1-DOF Layer Jamming Joint: Fig. 5 shows a sectional view of the assembled joint. The joint is assembled by hand. The flaps are cut via a laser cutting process. The upper and lower links are made of ABS plastic by a 3-D printing process. As shown in Fig. 4(b), there exist holes on two sides of the links where two fishing wires are passed through and tightened on both sides, therefore, pressing the upper links against the lower links to keep the two in contact. The flaps are glued together on each link and overlapped on top of each other with the pattern shown in Fig. 3. An elastomeric membrane is wrapped around the inside and outside of the assembled joint. The membrane is a latex rubber tube with a thickness of 0.2 mm. Flexible tubing is admitted into the membrane and connects to an external pump in order to supply a vacuum. O rings are used to fit the latex rubber onto the flexible tubing and the rigid links to achieve a vacuum seal. When vacuum pressure is applied, the air inside the membrane is drawn away, and the membrane applies a confining pressure to the outside flap surface. The pressure can be 101.3 kPA (1 atm) at maximum.

The process of making the customized latex rubber tube is as follows. The raw material that was employed was an abrasion-resistant natural latex film rubber with the desired thickness (0.2 mm), which is commonly available. Liquid latex rubber was also employed in a diluted form (with an equal volume of water). Flat cardboard was used as a mold. The width of the cardboard was determined based on the required diameter of the tube. A mold release was applied to the cardboard to prevent the latex film from sticking to the cardboard. The latex film was then wrapped around the cardboard. Afterward, the latex film was brushed with the diluted liquid latex on the overlapping sections of the film, to form a closed tube. Weight was placed on top of the overlapping film region, and then, a heat gun was used to heat the glued, overlapping area. The tube was left to dry for 24 h, and after that, the weight was removed, and the finished tube was rolled off of the cardboard.

3) Modeling of 1-DOF Layer Jamming Joint: The effect of a given flap at an arbitrary position on the rotational joint stiffness can be analyzed with the diagram shown in Fig. 6(a). For a 1-DOF rotational joint, the motion of a "side flap" (with the flap

This article has been accepted for inclusion in a future issue of this journal. Content is final as presented, with the exception of pagination.

face oriented normal to the axis of joint rotation) is rotational along the axis of the pivot, whereas motion of a "front flap" (with the flap face oriented parallel to the axis of joint rotation) is purely translational, as in Fig. 3. Intermediate flaps have combined motion of rotation and translation.

Considering two arbitrary points P_1 and P_2 on a flap face that have nonzero separation distance w', the amount of motion of the points caused by rotation θ of the joint can be calculated as follows:

$$\Delta m_1 = r \sin \phi_1 \, \Delta\theta$$
$$\Delta m_2 = r \sin \phi_2 \Delta\theta \tag{2}$$

where ϕ_1 and ϕ_2 denote the angles from the joint axis to each point, and r is the radius of the cylinder formed by the flaps. If w' is sufficiently small, it can be expressed as

$$w' \cong r(\phi_2 - \phi_1). \tag{3}$$

From (2) and (3), and by converting ϕ_1 and ϕ_2 to ϕ, which is the angle from the joint axis to a point on the flap, the rotational motion component $\Delta\psi$ and translational motion component Δm are obtained as follows:

$$\Delta\psi \cong \lim_{\phi_1,\phi_2 \to \phi} \frac{\Delta m_2 - \Delta m_1}{w'} = \cos\phi \Delta\theta \tag{4}$$
$$\Delta m \cong \lim_{\phi_1,\phi_2 \to \phi} \frac{\Delta m_2 + \Delta m_1}{2} = r \sin\phi \Delta\theta.$$

The relationship between the frictional force of the flaps and the resisting torque on the joint can be calculated by using the virtual work method. If a flap is sufficiently long, the motion Δv of an infinitesimal part of the flaps in Fig. 6(b) is as follows:

$$|\Delta v| = \sqrt{(l\Delta\psi)^2 + \Delta m^2} = \sqrt{(l\cos\phi)^2 + (r\sin\phi)^2}\Delta\theta. \tag{5}$$

In order to satisfy energy conservation, the following equation should hold:

$$\tau\Delta\theta = \int_{-\frac{L}{2}}^{\frac{L}{2}} |\Delta v| \, p \, \mu \, w dl = 2\int_{0}^{\frac{L}{2}} |\Delta v| \, p \, \mu \, w dl. \tag{6}$$

Substituting Δv into (6) with (5), the resisting torque $\tau(\phi)$ can be obtained as follows:

$$\tau(\phi) = 2p\,\mu\,w \int_0^{\frac{L}{2}} \sqrt{(l\cos\phi)^2 + (r\sin\phi)^2} dl \tag{7}$$
$$= p\,\mu\,w \left(\frac{L}{4}\sqrt{(L\cos\phi)^2 + (2r\sin\phi)^2} + \frac{(r\sin\phi)^2}{|\cos\phi|} \right.$$
$$\left. \times \ln\left(\frac{L}{2r}|\cot\phi| + \sqrt{\left(\frac{L}{2r}\cot\phi\right)^2 + 1} \right) \right).$$

From this equation, the total resisting torque of a 1-DOF layer jamming joint can be calculated as follows:

$$\tau_{1\,\mathrm{DOF}} = n \sum_{n_{\mathrm{flap}}} \tau(\phi). \tag{8}$$

where n_{flap} denotes the number of flaps around the cylindrical frame. Fig. 7 shows the change in resisting force of one flap as a function of the change of the angle ϕ, as computed from (7), where the radius of the cylinder r is 10 mm. All of the flaps of Fig. 7(a)–(c) have an identical size of 40 mm, although with widely varying aspect ratios. Note that $\phi = 0°$ represents the location of a front flap, and $\phi = 90°$ represents the location of a side flap.

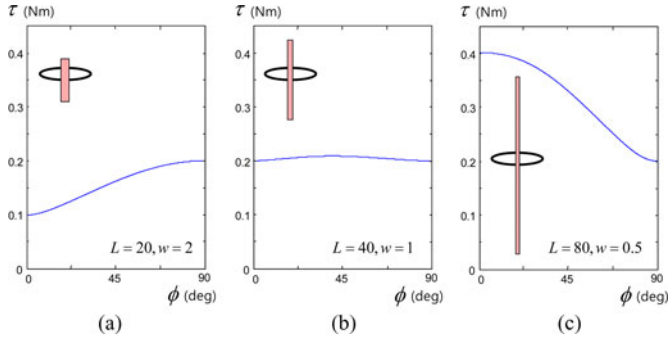

Fig. 7. Resisting torque comparison of three representative flaps geometries.

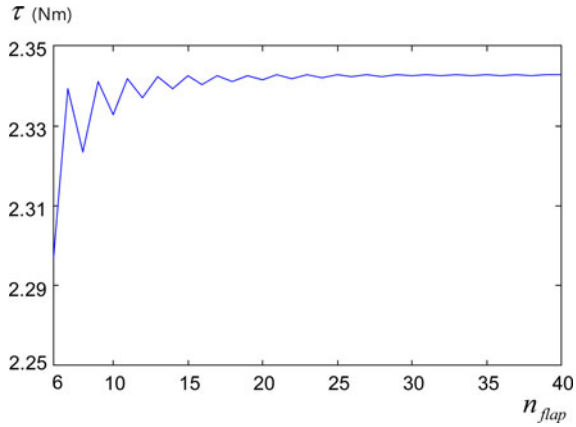

Fig. 8. Resisting torque variation according to the number of flaps around the frame.

When the length of the flap is four times longer than the radius of the cylinder [see Fig. 7(b)], the resisting force of the front flap is exactly the same as the side flaps, and the intermediate flaps contribute slightly more than either the front or side flap.

As shown in Fig. 7(c), the greatest contribution to resisting force is derived from a relatively long flap at the front position, which agrees with intuition. Also, the contribution of the side flaps does not change as a function of aspect ratio, which also agrees with intuition. It should be noted that, in practice, there is a geometric constraint on flap length caused by overlapping and interference of adjacent flaps during joint bending. In addition, another practical constraint derives from the fact that long flaps can be prone to buckling or creasing.

Fig. 8 represents the resisting torque according to the number of flaps n_{flap}, where the size of total contact surface remains constant, i.e., $n_{\mathrm{flap}} w =$ constant. Considering the scale of the y-axis of the graph, we can notice that the resisting torque is not changed significantly, and it converges to a constant value. The torque in the region of lower numbers of n_{flap} has small fluctuation. It is caused by the placement of the flaps around the frame. Fig. 8 was obtained assuming that the first flap is

This article has been accepted for inclusion in a future issue of this journal. Content is final as presented, with the exception of pagination.

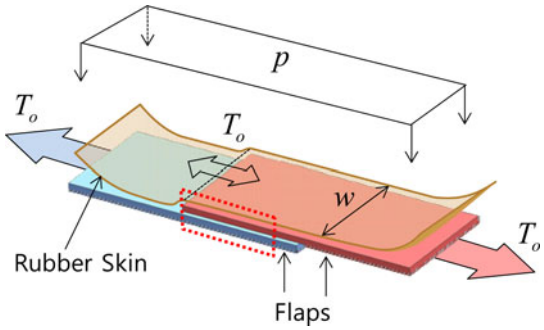

Fig. 9. Flaps and rubber skin movement.

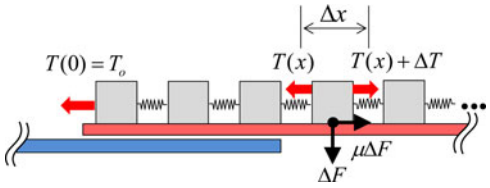

Fig. 10. Schematic of elastomeric membrane tension.

aligned with the pivot direction. If the position of the first flap is changed, the shape of fluctuation will be changed. Ideally, we can choose an arbitrary number of n_{flap} without losing resisting torque performance. However, if n_{flap} is extremely high, the width of the flaps w becomes too small to resist buckling and creasing, and in the opposite situation, an unnecessarily large flap width decreases the flexibility of the mechanism. Here, we have chosen n_{flap} between 8 and 12.

4) Modeling of Membrane Tension: Besides the friction between flaps in the layer jamming mechanism, the tension between the elastomeric membrane (here, latex rubber) and the flaps plays an important role in determining joint stiffness. The elastomeric membrane tends to resist relative movement when the flaps slide on top of one another. In order to better understand the mechanism, membrane tension was modeled analytically and validated by 3-D finite-element analysis (FEA) simulation.

Fig. 9 shows a diagram of two flaps covered by an elastomeric membrane moving in opposite directions, while subject to a confining pressure. Let us assume that the friction acts only between the flap and the membrane and that there is no friction between the flaps, and then, the tension T_0 of the membrane at the contacting edge between the two flaps (see black dotted line of Fig. 7) is the same as pulling force of each flap.

The elastomeric membrane can be represented as a number of lumped elements connected by springs, as illustrated in Fig. 10.

Here, ΔF is the confining force on the membrane and flap caused by the pressure p, and $\mu\,\Delta F$ is the corresponding friction force between the membrane and flap. Thus

$$F = pw\Delta x \tag{9}$$

$$T(x) = T(x) + \Delta T + \mu F. \tag{10}$$

From (9) and (10), we can obtain

$$\Delta T = -\mu F = -p\mu w\Delta x \tag{11}$$

where ΔT is the difference in tension across a small section of membrane Δx, and the boundary condition for this equation is $T|_{x=0} = T_0$. Therefore, the tension along the entire membrane can be obtained by integrating over the length x:

$$T(x) = \int_0^x \Delta T = \int_0^x p\mu w dx, \quad T(0) = T_o. \tag{12}$$

Since the membrane cannot take compressive force, $T(x)$ always has a positive value. Thus, the tension distribution along the membrane is

$$T(x) = \begin{cases} T_o - p\mu wx, & x < \dfrac{T_o}{p\mu w} \\ 0, & x \geq \dfrac{T_o}{p\mu w}. \end{cases} \tag{13}$$

What we are interested in is the relationship between the displacement of the two flaps and the tensile force of the flaps T_0. If we assume that L_t is the displacement of the two flaps, which is the same as total elongated length of the membrane, and based on Young's modulus definition, we can obtain

$$\frac{EA}{\Delta x}\Delta l_t = T \tag{14}$$

$$L_t = 2\int_0^{\frac{T_o}{p\mu w}} dl_t = 2\int_0^{\frac{T_o}{p\mu w}} \frac{T}{EA}dx \tag{15}$$

where Δl_t is infinitesimal elongation of the membrane in the region of Δx, and A is the cross-sectional area of the membrane. The elongation of a membrane occurs at the both sides of the contacting edge, and thus, L_t in (15) has a doubled value of the integral. Using (13) and (15)

$$\begin{aligned} L_t &= 2\int_0^{\frac{T_o}{p\mu w}} \frac{T}{EA}dx = 2\int_0^{\frac{T_o}{p\mu w}} \frac{T_o - puwx}{EA}dx \\ &= \frac{2}{EA}\left(T_o x - \frac{puw}{2}x^2\right)\Big|_0^{\frac{T_o}{p\mu w}} \\ &= \frac{2}{EA}\left(T_o\frac{T_o}{p\mu w} - \frac{puw}{2}\left(\frac{T_o}{p\mu w}\right)^2\right) \\ &= \frac{T_o^2}{EAp\mu w}. \end{aligned}$$

As a result, the membrane tension as a function of L_t is obtained as follows:

$$T_o = \sqrt{EAp\mu wL_t}. \tag{16}$$

We can also calculate the length of the region of nonzero tension by using (13) and (16):

$$x_{\max} = \frac{T_o}{p\mu w} = \sqrt{\frac{EAL_t}{p\mu w}}. \tag{17}$$

In order to better understand the tension distribution and effect of membrane physical parameters on the layer jamming mechanism performance, the membrane tension was modeled analytically. This model was then validated by 3-D FEA simulation.

This article has been accepted for inclusion in a future issue of this journal. Content is final as presented, with the exception of pagination.

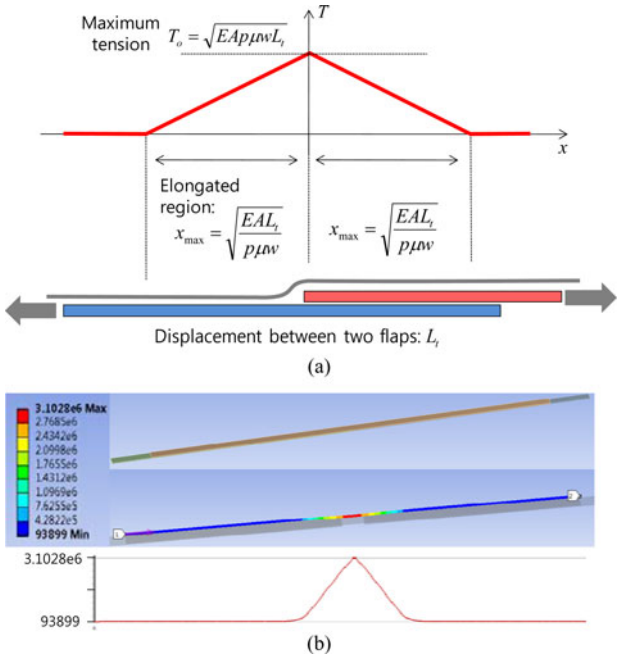

Fig. 11. Modeled membrane tension distribution.

It can be seen that the membrane tension increases linearly to a maximum value that occurs at the contacting edge of the top flap with the membrane. The maximum tension and the elongated length are determined by the Young's modulus of the membrane E, the cross-sectional area of the membrane A, the pressure acting on the membrane p, the friction coefficient of the flap material μ, the width of the flap w, and the contacting distance between two flaps L, as illustrated in (16) and (17).

Fig. 11(b) (bottom two) shows ANSYS simulation results of the stress distribution of the membrane. Ansys 13.0 workbench (static structure) was used. The width of both flaps and rubber was all 6 mm, the length of flaps was 60 mm each, the thickness of the flaps is 0.2 mm, the length of the rubber is 100 mm, the thickness of the rubber was 0.15 mm, and the frictional coefficient between flap and rubber was 0.5. The flaps were modeled as rigid and not stretchable. The rubber was selected as latex rubber with a Young's modulus set to 0.02 GPa and a Poisson ratio set to 0.5. The piecewise linear tension distribution from the FEA simulation (bottom two) closely matches the membrane tension distribution pattern computed from the analytical model. This serves as an initial validation of the theoretical modeling of the membrane tension distribution.

In the similar way as Fig. 9, a model of the membrane under shear stress can be obtained. Fig. 12 shows a diagram of two flaps under shear force S_o. The force distribution along the membrane is the same as (13), and the following deduction is also similar, except that the Young's modulus E should be substituted with shear modulus G. Therefore, assuming that L_s is the shear displacement between the flaps, the resultant membrane shear force as a function of L_s can be obtained as follows:

$$S_o = \sqrt{GAp\,\mu\,wL_S}. \tag{18}$$

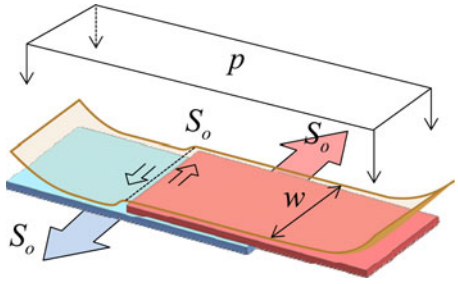

Fig. 12. Flaps and rubber skin movement under shear force.

Let us consider the relationship between rotation angle and the resisting torque of the joint. If we assume that the rotation is sufficiently small, the tensile motion L_t and the shear motion L_s of the flap edge can be calculated from (4) as

$$L_t \cong (r\sin\phi)\,\theta, \quad L_s \cong \left(\frac{L}{2}\cos\phi\right)\theta. \tag{19}$$

Again, by using virtual work concept to satisfy energy conservation and substituting (16), (18), and (19) into (20), shown below the following equation can be obtained:

$$\begin{aligned}\tau_m\Delta\theta &= T_o\Delta L_t + S_o\Delta L_s \\ &= \sqrt{EAp\,\mu\,w\,(r\sin\phi)\,|\theta|}\,(r\sin\phi)\,\Delta\theta \\ &\quad + \sqrt{GAp\,\mu\,w\left(\frac{L}{2}\cos\phi\right)|\theta|}\left(\frac{L}{2}\cos\phi\right)\Delta\theta. \end{aligned}\tag{20}$$

If we consider the nature of rubber material, we can notice that the membrane cannot make resisting force under compressive motion of the flaps; on the other hand, the shear motion in the both directions can produce resisting force. Therefore, the resisting torque caused by membrane elongation and shear is

$$\tau_m = \begin{cases} \left(\sqrt{EAp\,\mu\,w\,(r\sin\phi)^3} + \sqrt{GAp\,\mu\,w\left(\frac{L}{2}\cos\phi\right)^3}\right)|\theta|^{\frac{1}{2}} \\ \qquad\qquad 0 \le \phi \le \pi \\ \sqrt{GAp\,\mu\,w\left(\frac{L}{2}\cos\phi\right)^3}\,|\theta|^{\frac{1}{2}}, \qquad \pi < \phi < 2\pi. \end{cases}\tag{21}$$

From this equation, the total resisting torque of a 1-DOF layer jamming joint due to membrane can be calculated as follows:

$$\tau_{m1\,\mathrm{DOF}} = \sum_{\mathrm{flaps}} \tau_m(\phi). \tag{22}$$

Here, substantial approximation was applied because only the membrane mechanics at the edge of the flaps was considered, and the complex shape of whole flaps was ignored. However, it is notable that the membrane contributes the resisting torque then and not until then the flaps has relative displacement and the contribution has square root relation with the bending angle.

5) Characteristics of 1-DOF Layer Jamming: In order to validate the layer jamming model, bending stress tests were conducted on a physical prototype of the simple 1-DOF layer jamming joint described in Sections II-A and B.

This article has been accepted for inclusion in a future issue of this journal. Content is final as presented, with the exception of pagination.

TABLE I
SPECIFICATIONS AND TEST ENVIRONMENTS OF 1-DOF LAYER JAMMING JOINT

Specification	Value
Radius of the cylinder r,	10mm
Width of flaps w,	5 mm
Overlapped length of flaps L,	15 mm
No. of flaps per circle n_{flap},	10
No. of contact surface n,	7
Frictional coefficient μ,	0.60
Vacuum pressure p,	0, 33.3, 66.7, 101kPa

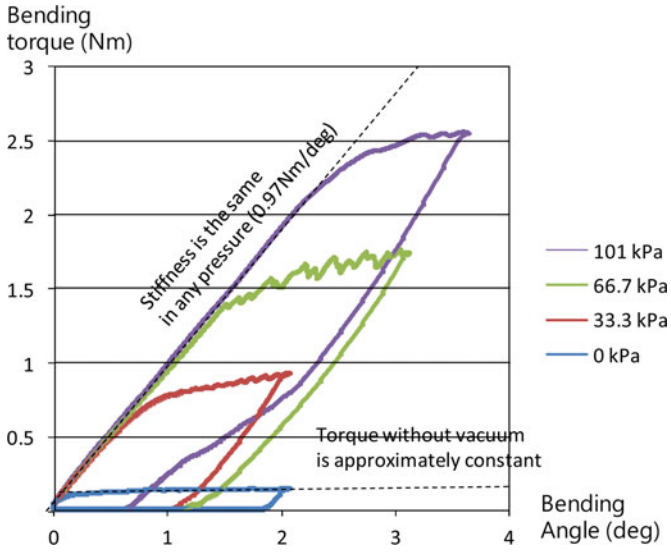

Fig. 13. Bending torque-angle curves of 1-DOF layer jamming joint.

Table I shows specifications of the 1-DOF layer jamming joint and the test environment. From these specifications and (7) and (8), the resisting torque can be calculated theoretically. The calculated resisting torque under 101 kPa (1 atm) vacuum pressure was calculated as 2.3 N·m.

Also it is clear from (1) that when n increases, the total resistant force is increased. The maximum number of layers n is limited by the thickness requirement of the tube and the stiffness requirement of the mechanism. The outer diameter of the tube is set to be 22 mm, which is smaller than the maximum umbilical incision diameter 40 mm. Inner diameter is 15 mm and is decided by outer diameter and thickness of flaps and rubber skin, which is enough for insertion of other flexible surgical tools.

Experiments to measure the stiffness properties of the 1-DOF joint were conducted by using a texture analyzer. The texture analyzer can simultaneously apply controlled bending forces to the endpoint of the joint while measuring endpoint displacement. The texture analyzer has a 49 N maximum force capability and 0.001 N sensitivity.

The experimental value measured by repeated stress test was found to range between 2.2 and 2.7 N·m, which agrees reasonably well with the theoretical value of 2.3 N·m.

Fig. 13 presents bending stress–strain curves under various vacuum pressures. Within the resisting torque range, it shows

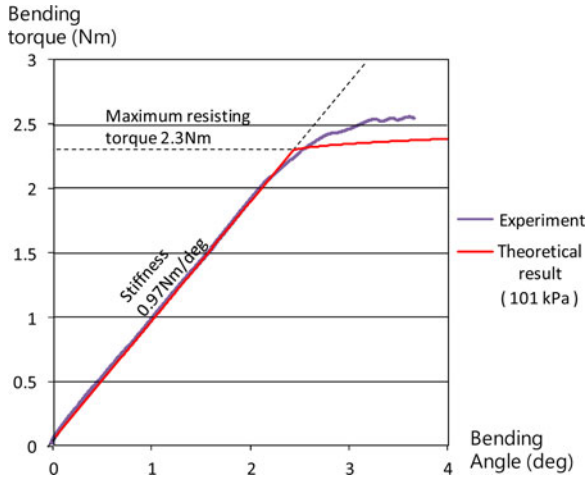

Fig. 14. Comparison between the theoretical and experimental results of bending torque-bending angle relationship.

a high linear stiffness (0.95 N·m/deg) that is independent of vacuum pressure level. This independence is due to the fact that failure (due to flaps sliding with respect to one another) occurs only when the shear force between individual flaps exceeds the friction limit; below this level, the flaps are effectively bonded to one another. Once the external torque exceeds the resisting torque, however, the curve becomes nonlinear. However, in contrast with a typical Coulomb friction curve which has approximately zero slope, the torque increases continuously as it bends, which is caused by the increasing resistant nonlinear bending force from the flaps and the membrane tension, as we derived in (21).

Fig. 14 shows the comparison between the experimental and the theoretical torque. The slope of the theoretical curve under resisting torque is adopted from the experimental result (0.97 N·m/deg), and it goes until the theoretical resisting torque (2.3 N·m) obtained by (8) and, above the resisting torque, the curve follows the torque provided by the membrane of (22). These curves have two distinct differences. First, the experimental curve does not exhibit a sharp inflection point near its maximum resisting torque, because all of the relative motion between flaps does not occur at the same time. Second, the experimental slope above the resisting torque shows greater stiffness. It is speculated that the resisting torque of the membrane comes not only from the end edge of the flaps but from the side edge of the flaps as well. If more precise identification of this is needed, precise modeling on whole edges of flaps should be conducted.

Note that the bending torque without vacuum pressure is a constant nonzero value, because the flaps without vacuum exhibit a finite level of friction. This gives insight into desirable characteristics of the film material. For instance, if the stiction of the material is extremely high, it will be difficult to achieve a high stiffness change, because the flaps will adhere to one another, even in the absence of vacuum pressure. In addition, the effect of the rubber membrane is negligible when it is not subject to vacuum pressure, because the membrane does not adhere to the flaps, and the stiffness of the membrane itself is

This article has been accepted for inclusion in a future issue of this journal. Content is final as presented, with the exception of pagination.

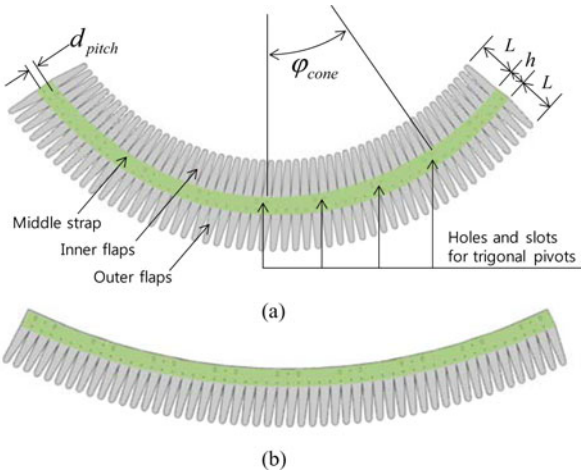

Fig. 15. (a) Double-side flap pattern for layer jamming manipulator having inner flaps and outer flaps. (b) Single-side flap pattern for layer jamming manipulator having outer flaps only.

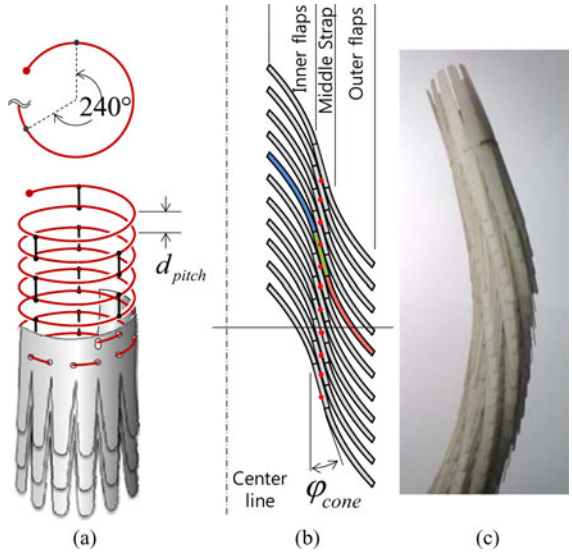

Fig. 16. (a) Assembled one-side flap pattern. (b) Section view of double side flap pattern. (c) Assembled double-side flap pattern.

very low. In addition, it also implies that the returning torque caused by flap flexion is almost 0, because the thickness of flaps is sufficiently thin enough to neglect the bending force of the flaps. However, if thicker flaps are chosen for other application, it should be considered in calculating the resisting torque.

III. Development of Tubular Snake-Like Manipulator With Layer Jamming

The 1-DOF layer jamming joint described above was intended to illustrate and model the basic functionality of the layer jamming mechanism. In this section, we introduce a new design concept for a tubular manipulator that is composed primarily of thin flap material, a latex membrane, monofilament wires, and flexible transmission rods. The manipulator provides large flexibility in a thin structure, while maintaining the tunable stiffness properties of layer jamming.

A. Construction of a Tubular Layer Jamming Structure

A flap pattern geometry suitable for a tubular manipulator is illustrated in Fig. 15. The patterns are composed of inner flaps or outer flaps (gray sections) and a middle strap (green section). Fig. 15(a) shows a double-side flap pattern for manipulators having both inner flaps and outer flaps; Fig. 15(b) shows a single-side flap pattern for manipulators having only outer flaps. The difference between the double-side and single-side flaps is that double-side flaps have flaps on each side of the middle strap: One flap lays on the outer surface of the tube, and the other flap lays on the inner surface of the tube, as shown in Fig. 16(b). Therefore, double-side flaps theoretically have up to twice the friction force compared with single-side flaps. For this reason, the layer jamming manipulator prototype described in this paper uses double-side flaps.

On the middle strap, there is a pattern of holes and slots, through which are woven a monofilament wire to constrain the tubular structure. Fig. 16(a) illustrates an assembled structure with a single-side flap pattern, where the woven wire (red curve) has a helical shape, and the pivots (black line) formed by holes and slots of the middle strap are evenly positioned at every 240° of the helical shape. Due to these pivots, in addition to the flexibility of film material, the tubular structure can be bent to an arbitrary angle as well as extended or shrunk in the axial direction.

The middle strap has a curved shape that forms a helical surface when rolled up. This enables it to stack without changing diameter, as shown in Fig. 16(b). By simple calculation, the gap T_{gap} between the helical surfaces can be obtained as follows:

$$T_{\mathrm{gap}} = \frac{\varphi_{\mathrm{cone}} d_{\mathrm{pitch}}}{2\pi} \tag{23}$$

where φ_{cone} is the inclination angle of the middle strap per winding. For actual implementation, T_{gap} should be larger than the thickness of the flap pattern T, since extra gap is required for the wire to allow room for bending. $\varphi_{\mathrm{cone}}, T$, and d_{pitch} used for implementation were 18°, 0.14 mm, and 6 mm, respectively. Therefore, T_{gap} was 0.3 mm, and the extra gap was 0.16 mm. As can be seen in Fig. 16(b), the length of flaps L, the height of middle strap h, and the pitch d_{pitch} determine the number of overlapped flaps n_{flaps} and that of overlapped middle strap n_{strap} as follows:

$$n_{\mathrm{flaps}} = L/d_{\mathrm{pitch}} \tag{24}$$

$$n_{\mathrm{strap}} = h/d_{\mathrm{pitch}}. \tag{25}$$

From (23)–(25), the total thickness of the tubular manipulator can be calculated as follows:

$$T_{\mathrm{tube}} = 2n_{\mathrm{flaps}}T + n_{\mathrm{strap}}T_{\mathrm{gap}}. \tag{26}$$

As L and h were 30 and 24 mm, respectively, the thickness of the tube is 1.9 mm. Adding the thickness of the latex rubber membrane for inside and outside sealing, the total thickness of the manipulator wall is 2.1 mm. This is a small value compared with other snake-like manipulators with tunable stiffness capability and, therefore, suggests that such a device could be useful

This article has been accepted for inclusion in a future issue of this journal. Content is final as presented, with the exception of pagination.

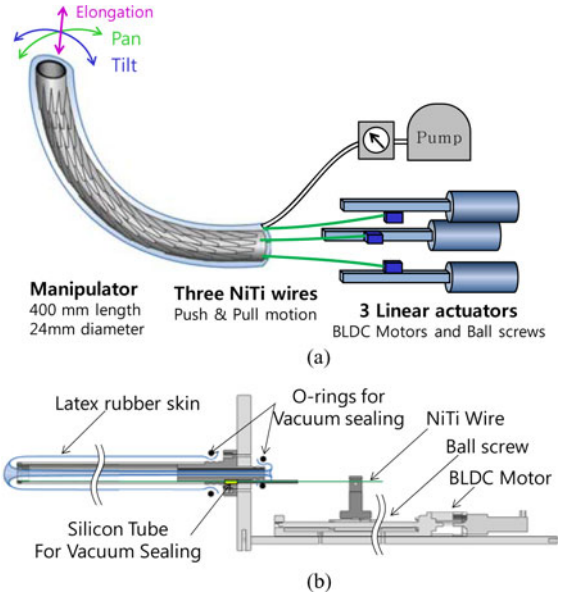

Fig. 17. (a) Concept design of layer jamming manipulator. (b) Section view of manipulator and one actuator.

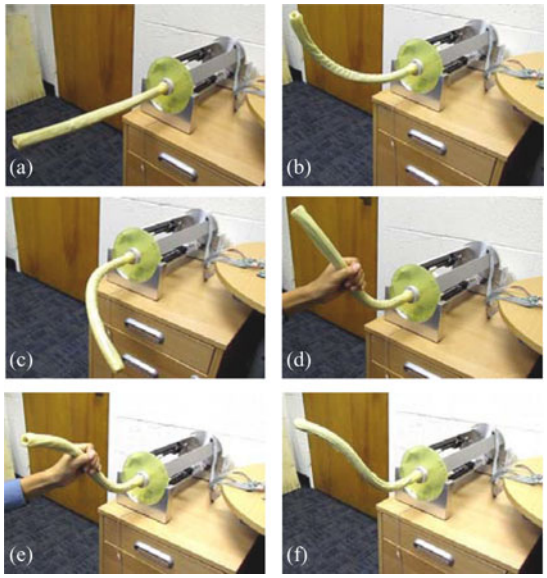

Fig. 18. Motion of layer jamming manipulator. (a)–(c) Free motion without vacuum. (d) and (e) Motion under external constraint without vacuum. (f) Stiffened state with vacuum.

for various MIS applications. Specifically, a thin, stiff device would be useful as a manipulable guide sheath for endoscopic tools.

B. Actuation and Transmission System

The actuation and transmission system of the manipulator is composed of transmission wires, linear actuators, and a vacuum system as shown in Fig. 17(a). In order to actuate the manipulator, three NiTi wires of 1 mm diameter were used for the transmission wires. They were placed at every 120° inside of the manipulator and passed through the loops made by film flaps and woven wires. Distal ends of the wires were fixed at the distal end of the tubular structure, and the proximal ends were connected to three linear actuators.

This approach is relatively simple and requires a small number of components. However, care must be taken in designing the device for vacuum sealing, because the sealing membrane must contain both the tubular structure and transmission wires. Placing the transmission wires outside the sealing membrane is desirable for a simple sealing design in the case when a thin structure is not needed. As shown in Fig. 17(b), silicon tubes were used for vacuum sealing of the transmission wires. To increase the sealing effect, Dow Corning high-vacuum grease silicone was applied inside the silicon tubes, which can also act as lubricant and reduce the friction in between the silicon tubes and the NiTi wires.

For actuation, three linear actuators were used. Each actuator is composed of a 1-mm pitch ball screw, linear guide, and 8-W brushless dc motor with a 5.4:1 gearhead. As the maximum continuous torque of the motor is 8 mN·m and the efficiency of the gearhead is 84%, the approximate continuous output force of the linear actuator is 230 N.

Fig. 17(b) shows a sectional view of the manipulator and one of the linear actuators. The length of the manipulator is 400 mm, and the length of actuation components is 430 mm. The assembly of the manipulator is also done by hand. Most parts, including the frame, motor holders, NiTi wires tightening stand, and others, are made of ABS plastics via 3-D printing. The flaps are made of Mylar sheets and cut via laser cutting. The latex rubber skin is made with the same manufacturing method as introduced in Section II. The NiTi wires are threaded through the flap trigonal pivot holes on each layer along the outside of the flaps and are glued onto only the top side of the manipulator. One latex membrane wraps inside and outside of the tubular manipulator and is sealed to one frame on both its top and bottom sides with two rubber O rings. The vacuum tube and transmission pass through the frame between the O rings. The NiTi wires are tightened onto the linear actuators via the tightening stands. The three linear actuators are mounted onto the frame by machine screws.

C. Characteristics of Tubular Snake-Like Manipulator With Layer Jamming

Fig. 18 shows several snapshots of motion of a tubular manipulator prototype under various conditions. The motion starts from a straight pose as shown in Fig. 18(a). As shown in Fig. 18(b) and (c), the manipulator without external force bends to approximately arc shapes. When subject to an external force, as shown in Fig. 18(d) and (e), the manipulator demonstrates compliant motion due to its underactuated structure. In an arbitrary shape, it can be stiffened via application of vacuum pressure, as shown in Fig. 18(f). Close examination of Fig. 18(f) shows that the elastomeric membrane is compressed tightly against the underlying layers, due to the application of vacuum pressure.

For quantitative performance characterization, tests similar to those reported on the 1-DOF layer jamming joint were

This article has been accepted for inclusion in a future issue of this journal. Content is final as presented, with the exception of pagination.

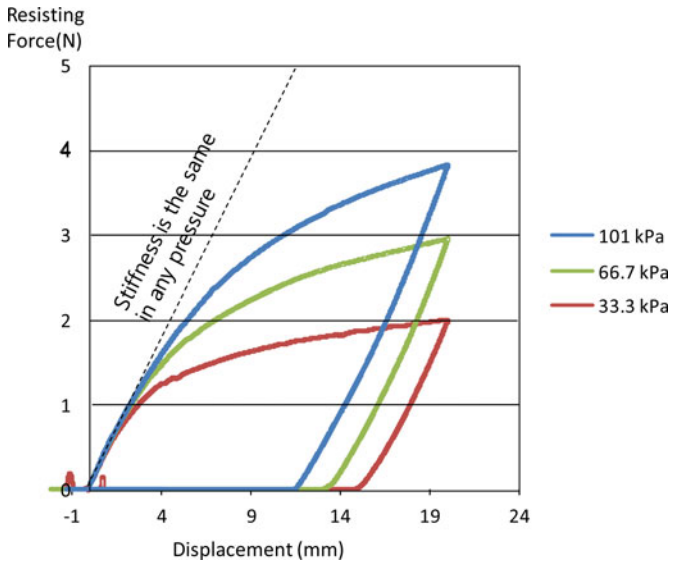

Fig. 19. Resisting force versus displacement curves of layer jamming manipulator.

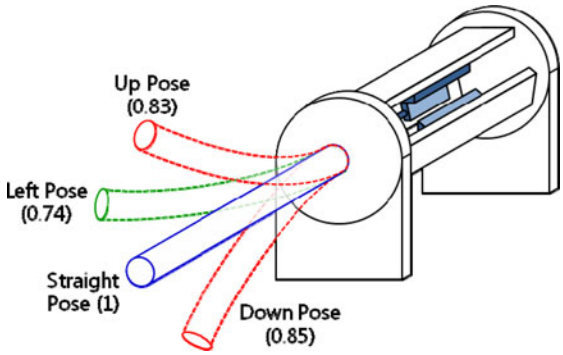

Fig. 20. Tube stiffness of the layer jamming manipulator at different poses.

conducted. A lateral (bending) force was applied at the tip of the manipulator, and applied vacuum pressures were the same as in Table I. The maximum breaking strength or resisting force is defined as the force where if it is released the manipulator would return to its initial pose. It is found out experimentally that the measured maximum resisting force under 101 kPa (1 atm) vacuum pressure was approximately 2 N, which indicates that the manipulator can bear a 2 N tip load, including its own weight and return to initial pose if the load is removed. Fig. 19 shows resisting force-displacement curves under various vacuum pressures. While the overall shape of the curves is similar to that of Fig. 13, the curve is generally smoother, and it is hard to differentiate a discrete failure point. This is due to the fact that the manipulator has more flexibility than the 1-DOF joint, and thus, there is more possibility of slippage between individual flaps, which results in a more gradual failure.

It was also observed experimentally that the bending stiffness of the tubular snake-like manipulator with layer jamming varies as a function of the manipulator pose. This effect is partly caused by the varying effect of gravity loading on the manipulator and partly by the deformation of the flaps and NiTi wires at various poses. Fig. 20 shows the stiffness of the manipulator at four poses: an upward pose, a downward pose, a straight pose, and a leftward pose. Due to symmetry, the rightward pose has the same stiffness as the leftward pose.

TABLE II
DDU Length Diameter and Payload Comparison

Devices	DDU Length (mm)	Outer Sheath Diameter (mm)	Payload (N)
IREP [1]	60	15	2
SPRINT [12]	142	30	5
LAYER JAMMING	400	22	2
DDES [4]	550	22	N/A
EndoSAMURAI [4]	1030	15.7	N/A
NOTES scope [4]	1330	14.3	N/A
IOP [4]	1100	18	N/A

MIS applications typically require that surgical manipulators should be able to have three controlled spatial DOFs. The manipulators should have high payload, high stiffness, and high resolution, with specific requirements dictated by the needs of particular surgeries. The required force for ordinary soft tissue surgery, such as needle insertion into the liver, has been stated as having a maximum of 2.5 N [20]. The payload of our prototype is about 2 N, and as it is explained previously in this paper, it can be easily increased by increasing the flaps numbers and contacting areas. Here, the desired stiffness of the proposed manipulator is 0.3 N/deg.

Table II compares the distal dexterity unit (DDU) length (not including surgical or manipulation tools like grippers or scissors), outer sheath diameter, and payload, for the layer jamming manipulator and some other MIS prototypes including IREP [1], SPRINT [12], and commercial products including DDES, EndoSAMURAI, NOTES scope, and IOP [4]. Due to the limited available data for some devices, the payloads of the commercial MIS products are not available. For MIS, DDU usually refers to robotic arms that start from a fixed entry port into patients' bodies, with attached surgical tools on the distal ends. The outer diameter of the prototype presented in this paper is 22 mm, with an inner diameter of 15 mm; however, it can be made smaller if the inner diameter is decreased.

Compared with these devices, the layer jamming manipulator has a relatively long length and small diameter, with a high payload. Furthermore, the payload of the layer jamming manipulator can be increased by increasing the number of layers, with a penalty of a small increase in the tube thickness, as shown in (1). Therefore, with the added advantage of tunable stiffness capability, this long, light, and very thin snake-like manipulator is very promising for MIS applications.

IV. Conclusion

This paper has introduced a novel layer jamming mechanism to achieve tunable stiffness in a compact articulated manipulator. Design, modeling, analysis, and experimental results of the

This article has been accepted for inclusion in a future issue of this journal. Content is final as presented, with the exception of pagination.

tubular layer jamming manipulator are presented. Experimental results demonstrate that the proposed mechanism has the capability of significant stiffness change and payload carrying capability, while it occupies a small volume. Therefore, the device could be well suited for MIS applications.

When vacuum pressure is not applied, the manipulator configuration can be controlled by actuating the Ni-Ti transmission wires, to guide the manipulator around obstacles to a desired location. The external surface of the manipulator is relatively compliant due to the use of an elastomeric membrane and, thus, is unlikely to cause damage to internal organs due to accidental contact. The manipulator can be used as a guide for other MIS tools or could potentially be used in concert with another variable stiffness manipulator. In this concept, two tubular manipulators would advance alternatively, one within the other, with the guiding tube in a high stiffness state, while the advancing is in a low stiffness state [15]. The performance of the device can be predicted with reasonable accuracy through the proposed analytical models.

For future research, quantitative friction modeling of the membrane and analysis of the optimal shape and thickness of the flaps will be investigated. Surveying and testing appropriate materials for the elastomeric membrane is another aspect of further research. It is hoped that this unique layer jamming mechanism will inspire various snake-like and flexible mechanisms with the aim to further improve surgical performance in MIS and, thus, will benefit patients.

REFERENCES

[1] J. Ding, K. Xu, R. Goldman, P. Allen, D. Fowler, and N. Simaan, "Design, simulation and evaluation of kinematic alternatives for insertable robotic effectors platforms in single port access surgery," in *Proc. IEEE Int. Conf. Robot. Autom.*, May 2010, pp. 1053–1058.

[2] C. Thompson, M. Ryou, N. Soper, E. Hungess, R. Rothstein, and L. Swanstrom, "Evaluation of a manually driven, multitasking platform for complex endoluminal and natural orifice transluminal endoscopic surgery applications," *Gastrointestinal Endoscopy*, vol. 70, no. 1, pp. 121–125, Jul. 2009.

[3] A. Degani, H. Choset, B. Zubiate, T. Ota, and M. Zenati, "Highly articulated robotic probe for minimally invasive surgery," in *Proc. Int. IEEE Eng. Med. Biol. Soc. Conf.*, Vancouver, BC, Canada, Aug. 2008, pp. 3273–3276.

[4] S. Shaikh and C. Thompson, "Natural orifice translumenal surgery: Flexible platform review," *World J. Gastrointestinal Surg.*, vol. 2, no. 6, pp. 210–216, Jun. 2010.

[5] I. Gravagne and I. Walker, "Manipulability, force, and compliance analysis for planar continuum manipulators," *IEEE Trans. Robot. Autom.*, vol. 18, no. 3, pp. 263–273, Jun. 2002.

[6] A. Petterssona, S. Davisb, J. O. Grayb, T. Doddc, and T. Ohlsson, "Design of a magnetorheological robot gripper for handling of delicate food products with varying shapes," *J. Food Eng.*, vol. 98, no. 3, pp. 332–338, Jun. 2010.

[7] J. Chen and W. Liao, "Design and control of a magnetorheological actuator for leg exoskeleton," in *Proc. IEEE Int. Conf. Robot. Biomimetics*, Sanya, China, Dec. 2007, pp. 1388–1393.

[8] N. Cheng, G. Ishigami, S. Hawthorne, C. Hao, M. Hansen, M. Telleria, R. Playter, and K. Iagnemma, "Design and analysis of a soft mobile robot composed of multiple thermally activated joints driven by a single actuator," in *Proc. IEEE Int. Conf. Robot. Autom.*, Anchorage, AK, USA, May 2010, pp. 5207–5212.

[9] M. Telleria, M. Hansen, D. Campbell, A. Servi, and M. Culpepper, "Modeling and implementation of solder-activated joints for single-actuator, centimeter-scale robotic mechanisms," in *Proc. IEEE Int. Conf. Robot. Autom.*, Anchorage, AK, USA, May 2010, pp. 1681–1686.

[10] E. Brown, N. Rodenberg, J Amend, A. Mozeika, E. Steltz, M. Zakin, H. Lipson, and H. Jaeger, "Universal robotic gripper based on the jamming of granular material," in *Proc. Nat. Acad. Sci. USA*, vol. 107, pp. 18809–18814, 2010.

[11] N. Cheng, M. Lobovsky, S. Keating, A. Setapen, K. Gero, A. Hosoi, and K. Iagnemma, "Design and analysis of a robust, low-cost, highly articulated manipulator enabled by jamming of granular media," in *Proc. IEEE Int. Conf. Robot. Autom.*, May 2012, pp. 4328–4333.

[12] P. Marco and S. Umberto, "Design of a novel bimanual robotic system for single-port laparoscopy," *IEEE/ASME Trans. Mechatronics*, vol. 15, no. 6, pp. 871–878, Dec. 2010.

[13] G. Dogangil, B. L. Davies, and F. R. Baena, "A review of medical robotics for minimally invasive soft tissue surgery," *Proc. Inst. Mech. Eng., Part H*, vol. 224, no. 5, pp. 653–679, 2010.

[14] B. W. Miedema, J. A. Astudillo, E. Sporn, and K. Thaler, "NOTES techniques: Present and future," *Eur. Surg.*, vol. 40, no. 3, pp. 103–110, 2008.

[15] Y. Chen, J. H. Chang, A. S. Greenlee, K. C. Cheung, A. H. Slocum, and R. Gupta, "Multi-turn, tension-stiffening catheter navigation system," in *Proc. IEEE Int. Conf. Rob. Autom.*, Anchorage, AK, USA, May 2010, pp. 5570–5575.

[16] Y. Kim, S. Cheng, S. Kim, and K. Iagnemma, "Design of a tubular snake-like manipulator with stiffening capability by layer jamming," in *Proc. Int. Conf. Intell. Robot. Syst.*, Portugal, Oct. 2012, pp. 4251–4256.

[17] S. Zuo, T. Ohdaira, K. Kuwana, Y. Nagao, S. Ieiri, M. Hashizume, T. Dohi, and K. Masamune, "Developing essential rigid-flexible outer sheath to enable novel multi-piercing surgery," in *Proc. Med. Image Comput. Comput.-Assist. Intervention*, 2012, pp. 26–33.

[18] M. Balasubramaniam, H. Dunn, E. Golaski, S. Son, K. Sriram, and A. Slocum, "An anti backlash two-part shaft coupling with interlocking elastically averaged teeth," *Precis. Eng.*, vol. 26, no. 3, pp. 314–330, Jul. 2002.

[19] M. Bureau, T. Keller, J. Perry, R. Velik, and Jan F. Veneman, "Variable stiffness structure for limb attachment," presented at the IEEE Int. Conf. Rehabil. Robot., Zurich, Switzerland, Jun. 29/Jul. 1, 2011.

[20] A. Okamura, C. Simone, and M. Leary, "Force modeling for needle insertion into soft tissue," *IEEE Trans. Biomed. Eng.*, vol. 51, no. 10, pp. 1707–1716, Oct. 2004.

Yong-Jae Kim received the M.S. and Ph.D. degrees in electrical engineering and computer science from the Korea Advanced Institute of Science and Technology, Daejeon, Korea, in 1998 and 2003, respectively.

He was a Principal Engineer with the Manufacturing Technology Center of Samsung Electronics, Korea. He is currently a Research Staff Member with the Samsung Advanced Institute of Technology, Yongin si, Korea. His research interests include electromechanical design and control of hyper-redundant robots and humanoid robots and physical human–machine interaction.

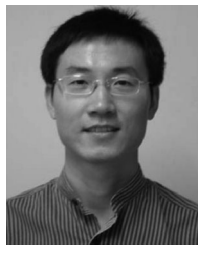

Shanbao Cheng received the B.S. and M.S. degrees from Sichuan University, Sichuan, China, and the Ph.D. degree from Nangyang Technological University, Singapore.

He is currently a Control Engineer with the Direct Drive System, FMC Technologies, Fullerton, CA, USA. In 2011, he was a Postdoctoral Researcher with the Massachusetts Institute of Technology, Cambridge, MA, USA, doing research on minimally invasive surgical robotics with variable stiffness. From 2008 to 2011, he was a Postdoctoral Researcher with the Rochester Institute of Technology, Rochester, NY, USA, developing magnetically levitated blood pumps. His research interests include minimally invasive surgical robotics, magnetic bearings, artificial heart pumps, permanent magnet synchronous motor control, and rotor-dynamics analysis.

This article has been accepted for inclusion in a future issue of this journal. Content is final as presented, with the exception of pagination.

Sangbae Kim received the B.S. degree from Yonsei University, Seoul, Korea, in 2001 and the M.S. and Ph.D. degrees from Stanford University, Stanford, CA, USA, in 2004 and 2008, respectively, all in mechanical engineering.

He is currently the Director with the Biomimetic Robotics Laboratory and an Assistant Professor of mechanical engineering with the Massachusetts Institute of Technology, Cambridge, MA, USA. He is involved in the convergence of mechanical engineering, control, biology, and material science. His achievement on bioinspired technology development includes the world's first directional adhesive based on gecko lizards and a climbing robot, called Stickybot, that utilizes the directional adhesives to climb smooth surfaces. Stickybot was featured as one of the best inventions of 2006 by TIME magazine, and the papers on Stickybot won the Best Paper Award for the TRANSACTIONS ON ROBOTICS 2008 and at the IEEE International Conference on Robotics and Automation in 2007. His research focuses on design process extracting principles from complex biological systems to achieve legged locomotion in engineering. He is currently focusing on a cheetah-inspired robotic platform capable of high-speed gallop, employing principles from quadrupedal runners.

Karl Iagnemma received the B.S. degree from the University of Michigan, Ann Arbor, MI, USA, and the M.S. and Ph.D. degrees from the Massachusetts Institute of Technology (MIT), Cambridge, MA, USA.

He was a National Science Foundation Graduate Fellow with MIT. He is currently a Principal Research Scientist and the Director of the Robotic Mobility Group MIT. He is author of the monograph *Mobile Robots in Rough Terrain: Estimation, Planning and Control with Application to Planetary Rovers* (New York, NY, USA: Springer, 2004) and coeditor of books on the Defense Advanced Research Projects Agency (DARPA) Grand Challenge and Urban Challenge autonomous vehicle competitions. He has authored or coauthored nearly 100 conference and journal papers on a wide range of robotic topics. His primary research interests include design, sensing, motion planning, and control of mobile robots in challenging environments.

Dr. Iagnemma has served as an Associate Editor of the IEEE TRANSACTIONS ON ROBOTICS and the *Journal of Field Robotics*. He recently led research programs for organizations including the U.S. Army Tank-Automotive and Armaments Command, the Army Research Office, DARPA, the NASA Mars Program Office, Ford Motor Company, Nissan, and Samsung, among others.